Journal of the Mechanics and Physics of Solids 79 (2015) 134–156

Contents lists available at ScienceDirect

Journal of the Mechanics and Physics of Solids

journal homepage: www.elsevier.com/locate/jmps

An experimental study on spontaneous adiabatic shear band formation in electro-magnetically collapsing cylinders

Z. Lovinger [a,b,*], D. Rittel [a], Z. Rosenberg [b]

[a] Faculty of Mechanical Engineering, Technion, Haifa 32000, Israel
[b] RAFAEL, P.O. Box 2250, Haifa 21031, Israel

ARTICLE INFO

Article history:
Received 4 January 2015
Received in revised form
5 April 2015
Accepted 11 April 2015
Available online 15 April 2015

ABSTRACT

The formation of shear bands in collapsing thick-walled cylinders (TWC) occurs in a spontaneous manner. The advantage of studying spontaneous, as opposed to forced, shear localization, is that it highlights the *inherent susceptibility* of the material to adiabatic shear banding without prescribed geometrical constraints. In the case of spontaneous shear localization, the role of microstructure (grain size and grain boundaries) on localization, is still unresolved. Using an electro-magnetic set-up, for the collapse of thick-walled cylinders, we examined the shear band formation and evolution in seven metallic alloys, with a wide range of strength and failure properties. To assess microstructural effects, we conducted systematic tests on copper and Ti6Al4V with different grain sizes. Our results match quite well with previously reported data on much larger specimens, showing the absence of a size effect, on adiabatic shearing. However, the measured shear band spacings, in this study, do not match the predictions of, existing analytical models, indicating that the physics of the problem needs to be better modeled.

1. Introduction

Shear localization is an important and often dominant failure mode at high strain rates, acting as a precursor to catastrophic failure (Bai and Dodd, 1992). The formation of an adiabatic shear band (ASB) in a dynamically loaded metal is viewed as a structural and/or material instability. The strength evolution of a material is controlled by two opposing mechanisms: hardening, such as strain and strain-rate hardening, and softening such as thermal (Zener and Hollomon, 1943; Davidenkov and Mirolubov, 1935) and microstructure-related softening (Rittel et al., 2006; Osovski et al., 2012). The classical approach of Zener and Hollomon (1943), found recently (Dodd et al., 2015) to be earlier presented by Kravz-Tarnavskii (1928) and Davidenkov and Mirolubov (1935), relates the initiation of adiabatic shear localization to the dominance of the thermal softening over the hardening mechanisms. Namely, under high rate deformation, the thermal softening results in a loss of strength which leads to a feedback mechanism between the plastic work and the consequent decrease in flow stress. This is a simple mechanism but one can argue that it is questionable since, as the material softens, it also generates less heat. In the last decade, an alternative process was proposed for ASB formation (Osovski et al., 2012; Rittel et al., 2008), identifying microstructural evolution (dynamic recrystallization) as the dominant mechanism. In these works, the dynamic stored energy of cold work is identified as the driving force for shear localization, which is, in fact, *preceded* and *triggered* by dynamic recrystallization (Rittel et al., 2006).

* Corresponding author at: Faculty of Mechanical Engineering, Technion, Haifa 32000, Israel.
E-mail address: cvloving@gmail.com (Z. Lovinger).

http://dx.doi.org/10.1016/j.jmps.2015.04.007
0022-5096/

The initiation and growth of shear bands have been extensively studied since the pioneering work of Zener and Hollomon (1943), using various experimental techniques with which the formation of a shear band is well defined. The Kolsky-bar technique is widely used for the study of shear localization with specially designed shear specimens, such as the "Hat" (Meyer and Manwaring, 1986) and "Punch" (Dabboussi and Nemes, 2005) geometries, or the Shear Compression Specimen (SCS) (Dorogoy and Rittel, 2005a, 2005b). The torsion bar is used to induce ASB in tubular specimens. This technique was used in the seminal work of Marchand and Duffy (1988), who identified the successive stages in the evolution of the adiabatic shear bands. Other experiments used pre-notched plates with a symmetric double notched specimen, as in Kalthoff and Wrinkler (1987), or an eccentric single notched specimen, as in Mason et al. (1994) and Zhou et al. (1996a, 1996b). In this set-up, the single or double notched plate is impacted by a projectile, causing a dominant mode II shear load. The shear bands initiate at the root of the notches, and their propagation is examined for various impact velocities. The common basis for all of these well-used techniques is that they all refer to a state of *forced* shear localization. In such cases, shear bands are formed in *well-defined regions*, dictated by the specimen geometry, parallel to the direction of the maximum shearing load. A controlled shear band has many advantages, enabling one to study the evolution of the shear localization process. Yet, the process of shear initiation is in fact dictated geometrically, and therefore externally forced.

In order to examine the initiation stage of shear localization, a different set-up is used, referring to *spontaneous* shear localization (as referred to by Chen et al. (1999)). In this case, the loading characteristics do not constrain the specific locations or directions of shear banding and multiple shear bands can evolve in regions and in directions other than the direction of the prescribed load. The major advantage of examining spontaneous shear localization is that it highlights the inherent susceptibility of the material to adiabatic shear banding.

The evolution of shear bands in the collapse of a thick-walled cylinder is an excellent example for spontaneous shear localization. In this case, an external pressure induces an inward collapse of the cylinder. The cylindrical symmetry lacks a transverse boundary, and shear bands which evolve from the inner surface of the collapsing cylinder, do not form on a clear boundary or by stress concentration. Free of transverse boundary constraints, the initiation of the shear bands occurs spontaneously. Nesterenko and Bondar (1994) and Nesterenko et al. (1989) introduced a well-controlled and repeatable technique to create multiple shear bands in collapsing thick walled cylinders, which is most suitable to study the properties and evolution of spontaneous ASB's. The Thick Walled Cylinder (TWC) is sandwiched between two cylindrical copper shells, which are driven inwards by an explosive cylinder, while the outer and inner copper shells control the extent of collapse of the sample. The diagnostics of this technique are post-mortem: the recovered sample is cut and polished to reveal the shear bands in the specimen. This technique has been used for various materials such as stainless steel (Xue et al., 2004; Meyers et al., 2003), CP Titanium and Ti6Al4V (Xue et al., 2002), aluminum alloys (Yang et al., 2008, 2009), ceramics (Espinosa and Gailly, 2001) and reactive materials (Nesterenko et al., 1994). Stokes et al. (2001) conducted several TWC experiments on the Pegasus-II facility using electro-magnetic forces as the driving collapsing force. A pronounced advantage of this loading technique is due to the more uniform collapse of the specimen, as compared with the explosively driven ones, which are also driven by an axial force due to the directional ignition of the explosive driver. More recently, we introduced an electromagnetically driven version of the TWC technique (Lovinger et al., 2011), using a pulsed current generator. This method has the advantage that it is highly controllable and somewhat simpler than the use of explosives or alternatively, the use of a large scale Mega-Joule energy facility.

In a TWC experiment, one can measure the number, spacing and length of the spontaneously initiated ASBs, as in Xue et al. (2004) and Lovinger et al. (2011). Consequently, the TWC techniques, either explosive or electromagnetic, offer an ideal experimental platform to validate existing models for ASB formation, and use the data to calibrate material models for shear band formation and patterning.

Several theoretical predictions of the spacing of shear bands can be found in the literature, such as those of Grady (1982), Grady and Kipp (1987), Wright and Okendon (1996) and Molinari (1997). These works are based on two main approaches to address the shear band phenomenon. Grady (1982) was the first to propose a perturbation solution for shear instability. This approach ties the mathematics of perturbations with the physical phenomena, suggesting that shear bands evolve at a spacing which is determined by minimum energy considerations, matching a dominant wave number, which is revealed by the perturbation calculation. Accounting for a viscous constitutive equation and linear thermal softening, Grady (1982) reached the following expression for the spacing, L_G, between shear bands:

$$L_G = \frac{2\pi}{\dot{\gamma}_0}\left[\frac{kC}{\alpha^2\tau_0}\right]^{1/4} \tag{1}$$

where k is the thermal conductivity, α is the thermal softening coefficient,[1] $\dot{\gamma}_0$ is the strain rate, C is the heat capacity and τ_0 is the shear flow stress at quasi-static conditions.

Later works by Wright and Okendon (1996), and by Molinari (1997) addressed this issue with a similar approach, by extending the materials' constitutive law to include rate dependency (Wright and Okendon, 1996) and strain hardening (Molinari, 1997). In these analyses the following expressions can be found.

[1] The thermal softening coefficient is defined for all models as $\alpha = \left.\frac{d\tau}{dT}\right|_{\varepsilon,\dot{\varepsilon}}$.

The band spacing according to Wright and Okendon (1996), is given by

$$L_{WO} = 2\pi\left[\frac{m^3 kC}{\dot{\gamma}_0^3 \alpha^2 \tau_0}\right]^{1/4} \tag{2}$$

while, according to Molinari (1997), using a constitutive model with linear thermal softening and power law strain hardening (with power n), the spacing is given by

$$L_{Mo} = 2\pi\left[1 - \frac{3}{4}\frac{\rho C}{\beta\tau_0^2}\frac{n(1-\alpha T)}{\beta\alpha\gamma}\right]^{-1}\left[\frac{m^3 kC(1-\alpha T_0)^2}{(1+m)\dot{\gamma}_0^3\alpha^2\tau_0}\right]^{1/4} \tag{3}$$

For a non-hardening material ($n=0$) Molinari's model takes the following form:

$$L_{Mo} = 2\pi\left[\frac{m^3 kC(1-\alpha T_0)^2}{(1+m)\dot{\gamma}_0^3\alpha^2\tau_0}\right]^{1/4} \tag{4}$$

The spacing expressions of Wright and Okendon (1996) in Eq. (2) and that obtained by Molinari (1997) in Eq. (4) show similar dependencies on strain hardening (power of 3/4), thermal conductivity (power of 1/4), heat capacity (power of 1/4) and strain rate (power of $-3/4$).

The second basic approach, due to Grady and Kipp (1987), extends Mott's (1947) analysis for dynamic fracture and fragmentation to shear banding. As Mott suggested, the velocity of the stress release wave is controlled by momentum diffusion. The momentum diffusion results with stress relaxation between evolving shear bands and the spacing expression is obtained by minimizing the localization time during which the shear band reaches a critical width. The spacing is then given by

$$L_{GK} = 2\left[\frac{9kC}{\dot{\gamma}_0^2\alpha^2\tau_0}\right]^{1/4} \tag{5}$$

using the same notations as above.

The predictions of these models were compared with experimental spacings in TWC tests in Meyers et al. (2003), Xue et al. (2002, 2004), Lovinger et al. (2011), Lovinger and Partom (2009). Significant differences are found between the predictions from the two approaches: the perturbation approach matches better the initiation stage of the shear bands, while the model of Grady and Kipp (1987) matches better the spacing between fully developed shear bands. The explanation for this difference is quite clear considering the derivation of the two models: the perturbation approach searches for a basic spatial frequency at which the shear bands will initiate. On the other hand, Grady and Kipp's approach is based on energy and momentum considerations, which are relevant to the mature stage of the developed shear bands, with a defined width and a reduced load bearing capacity. The comparison between the theoretical predictions and the experimental results shows the right order of magnitude agreement for both stages of initiation and of fully developed bands. Yet, quantitative comparison is still off by a factor of 3–4. Xue et al. (2004) addressed this gap by considering two-dimensional effects related to the interaction between shear bands, during their evolution process. The models, based either on perturbation analyses or momentum diffusion, assume that the thermal softening mechanism drives the material instability, accountable for the shear localization. The limited comparison in the literature does not enable a comprehensive elucidation of what defines the spacing between shear bands, and whether the thermal softening mechanism is in fact the dominant factor for the evolution of shear bands and their spatial distribution.

Beyond purely mechanical considerations, such as those mentioned above, one may consider the role of the microstructure of the material (grain-size and shape), as the initial geometrical perturbation for the initiation process. Answers to this issue are both relatively scarce and contradictory. On the one hand Xue et al. (2004) examined the influence of grain-size on the spacing in SS304L stainless steel using TWC specimens with grain sizes of 30–280 μm. They found the same spacing for all grain-sizes, even for the maximum grain-size, which exceeded the spacing distance. On the other hand, Bondar and Merzhievskii (2006), who examined the evolution of shear bands in TWC experiments with copper specimens having different grain sizes, reported a strong dependence of shear band initiation and evolution on grain size. Their experimental results showed that the critical strain for localization was much smaller for the coarse-grained material in comparison with the fine-grained one.

The measured values of the band spacing (Xue et al., 2004) and critical strains for localization (Bondar and Merzhievskii, 2006) in these two works are different, and do not enable a quantitative comparison. However, the conclusions from those two works are contradictory and call for a re-assessment of the influence of the microstructure on shear bands spacing.

Consequently, from the above literature survey, it appears that

(1) A sufficiently large database for the spacing of ASB's is still missing.
(2) The variety of investigated materials is still somewhat limited.

(3) A clear validation or possibly, further examination of the predictive analytical models for spacing between shear bands is still needed.
(4) Finally, the influence of the material's microstructure on the shear localization process remains to be elucidated.

The purpose of our work is to address these four points. The present paper is essentially experimental, introducing briefly the experimental setup, the various investigated materials and their microstructural and mechanical characteristics. This is followed by the experimental results about the distribution of the ASB spacing, namely their length distribution and numbers, for seven metallic alloys. These are compared with available data in the literature and with the above-mentioned analytical models.

2. Experimental set-up

We developed an electro-magnetic (EM) setup to provide the collapsing force on the cylindrical specimen, which was presented in detail in Lovinger et al. (2011), and so the following is only a brief summary. The EM setup is based on a pulsed current generator (PCG) using a 35 μF capacitor bank system. The capacitors are charged to voltages of 20–30 kV, which are released by using an array of low inductance rail spark-gaps, allowing a fast and simultaneous discharge into the conductor system. The currents created are of the order of 1–2 MA, with a typical rise-time of $\sim$1 μs. The conductor system is made of two plates, each attached to an opposite pole, separated by an isolating layer. The specimen is an assembly of coaxial cylinders: an inner Cu cylinder (inner diameter 3.1 mm, outer diameter 3.5 mm), the cylinder of the tested material (inner diameter 3.5 mm, outer diameter 5.0 mm), an outer Cu cylinder (inner diameter 5.0 mm, outer diameter 5.5 mm), attached to the upper conductor plate, an insulating plastic cylinder and an external cylinder made of brass (attached to the lower conductor plate). When the voltage is discharged, a current flows on both sides of the plastic isolator: on the internal boundary of the external cylinder and the internal boundary of the outer copper cylinder, but in opposite directions, thus creating repulsive magnetic forces between them. The external cylinder is driven outwards by expansion and the internal assembly of cylinders is collapsing inwards. The controllable parameters in the set-up are the charging voltage of the capacitors, resulting in different magnetic pressures, and the specimen's geometry, controlling the extent of collapse which determines the stage of shear band evolution.

The main diagnostics is post-mortem: the collapsing specimens, which come to a stop at the end of the experiment, are cut and polished to reveal the spatial distribution of shear bands and the spacing and lengths of the bands are measured. We use a B-dot probe (Lovinger et al., 2011) to assess the time history of the current-flow, in order to calculate the magnetic pressure. We use this also as the driving pressure in numerical simulations we are conducting to reconstruct the experimental results.

2.1. Experimental considerations on uniformity and repeatability

In order to establish the reliability of the results obtained with the experimental set-up, we carefully examined two important issues:

(1) The lengthwise uniformity of the collapsing process.
(2) Test repeatability.

The importance of these two issues is in assuring that the measured shear band distribution is not related to the specific cross-section we chose along the specimen to analyze the shear bands. In other words, show the universality of the results and their repeatability with several tests.

2.1.1. Uniformity of collapse

The lengthwise uniformity of the collapse process has been demonstrated in the explosively driven experiments by processing different cross sections cut from a single specimen and examining the number of shear bands and their spatial distribution (Chen et al., 1999; Nesterenko and Bondar, 1994; Nesterenko et al., 1989). Despite the pronounced directionality in these experiments, the uniformity was found to be very good, with small variance between adjacent cross sections. The collapse of the EM driven specimens was visually very uniform. In some of the specimens, the shear bands reached the external boundary, resulting in external "jigsaw" features (e.g in Ti6Al4V as shown later). These features were evident along the entire length of the specimens.

Nevertheless, we closely examined a SS304L specimen, by three different cross sections along its length, comparing the number of shear bands and their distribution in each cross section. Fig. 1 shows the comparison between these cross sections: the shear bands are evident at the inner boundary as a "jigsaw" pattern. The number of shear bands was very close in all three cross-sections (50–52). To compare the shear band distribution we examined the empirical cumulative distribution function (ECDF) (Lovinger et al., 2011) as a quantitative measure we chose to use. Evidently, the ECDF for the three cross-sections compare well and are within the lower and upper boundaries of the ECDF estimation.

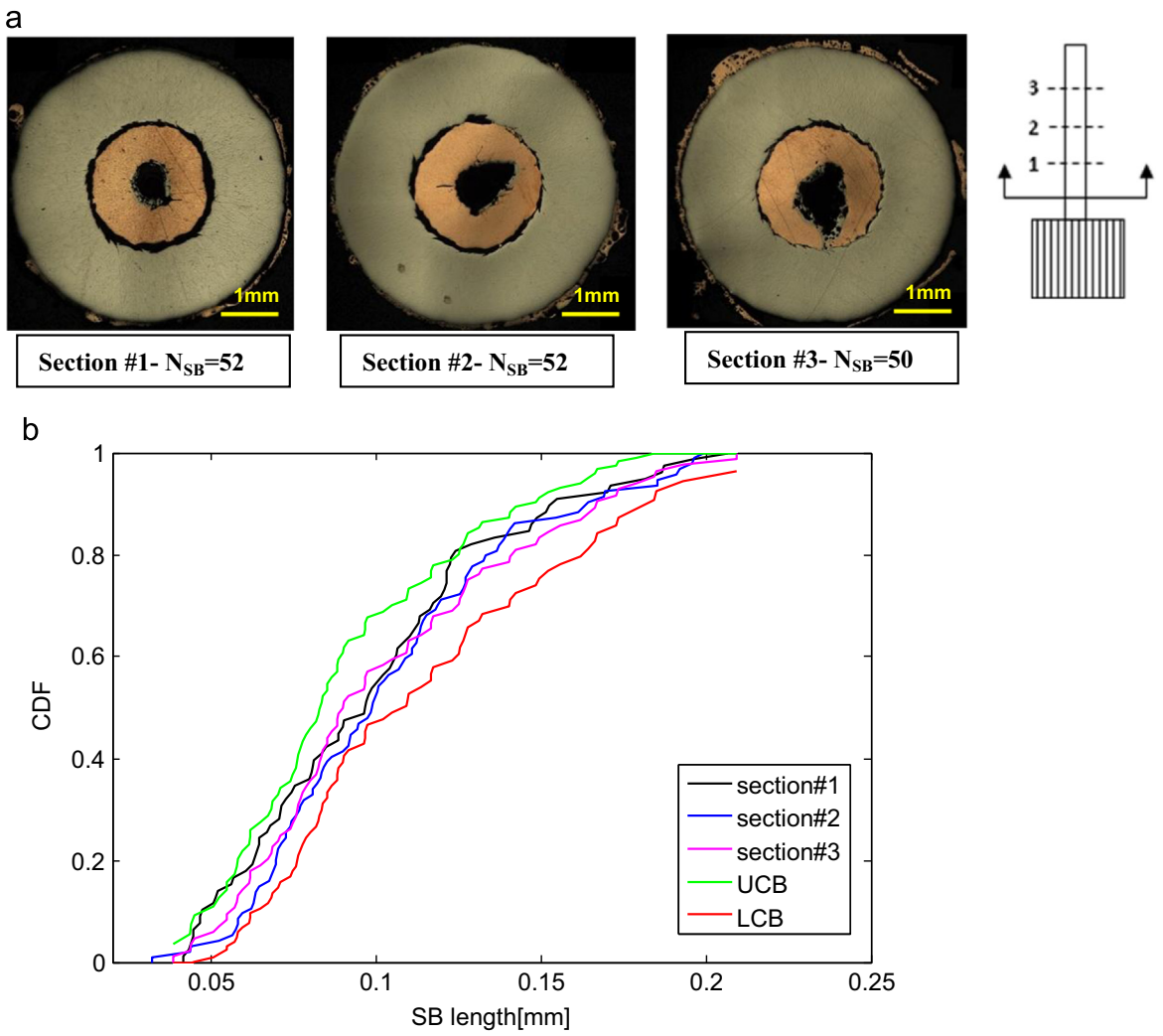

Fig. 1. Uniformity of collapse in a SS304L specimen: (a) micrographs of the three cross sections and (b) shear band distribution in the three cross sections using the ECDF measure for comparison (Lovinger et al., 2011).

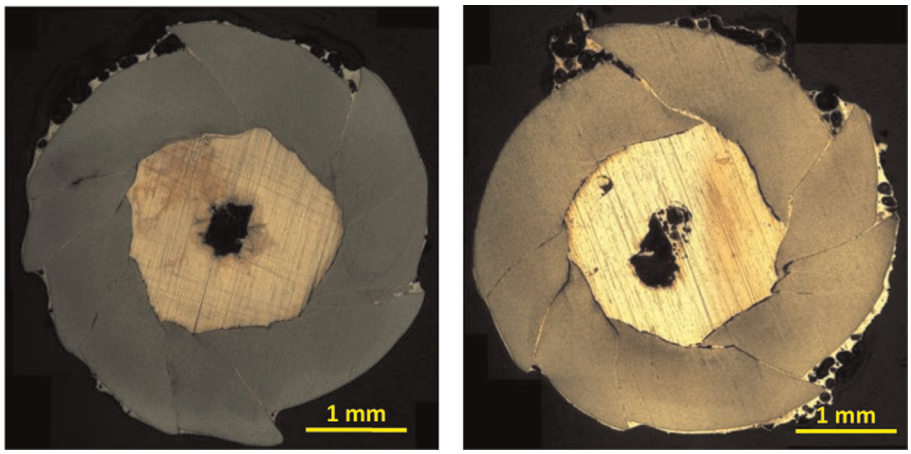

Fig. 2. A demonstration of repeatability of tests on the EM set-up: two specimens of wrought Ti6Al4V having the same geometry and the same loading conditions, showing similar behavior and number of shear bands.

To summarize, the lengthwise uniformity of the collapsing EM driven specimens was found to be very good.

2.1.2. Repeatability

Repeatability was examined by repeating tests with the same geometry and loading conditions and was found to be very good. An example of the quality of these repeated tests is shown in Fig. 2, for wrought Ti6Al4V specimens.

To summarize, the experimental set up was established as a controllable and repeatable technique for studying the evolution of multiple shear bands in collapsing cylinders. This set up enables one to conduct large numbers of experiments in a laboratory facility, with relatively low costs and high throughput of 2–3 tests a day. This is a significant improvement compared with the explosively driven technique. We used this experimental set-up to conduct about 40 tests on various materials to examine the evolution of spontaneous shear bands in different materials and to examine the effect of grain size on shear band initiation, as presented next.

3. Tested materials

Using the EM set-up described above, we conducted tests on seven materials:

(1) Stainless steel – ss304L.
(2) Titanium (CP grade2).
(3) Ti6Al4V – wrought material.
(4) Ti6Al4V – fabricated by LMD (Laser metal deposition – "printed" material).
(5) Cast aluminum alloy Al-A356.
(6) Cast magnesium alloy Mg-AM50.
(7) OFHC Copper – heat treated copper with variable grain size (to assess the effect of grain-size on shear band distribution).

The dynamic strength of each of the tested materials was characterized by tests on our Kolsky bar system (Split-Hopkinson pressure bar). Characteristic stress–strain curves from these tests are shown in Fig. 3. Strain rates in these tests were 3000–5000 s^{-1}

The different tested materials cover a large span of strength and ductility. The first three materials listed above – SS304L, CP-Ti and Ti6Al4V – were previously studied in the explosively driven experiments, and they were used to compare our results with those reported in the literature (Xue et al., 2002, 2004; Meyers et al., 2003). The additional materials were selected for the following reasons:

(1) LMD-Ti6Al4V – was chosen to examine the influence of microstructure and grain size, in comparison with the wrought Ti6Al4V.
(2) OFHC Copper with different grain sizes – was chosen to systematically examine the influence of grain size, with reference to the work of Bondar and Merzhievskii (2006).
(3) MgAM50 has a similar behavior as Ti6Al4V, as both materials experience failure at low strains (~20%) in the Kolsky-bar tests.
(4) Al-A356 was chosen as a very different material, with low tensile ductility (3.5% failure strain in tension), although in compression it showed a very high ductility, close to that of copper as shown in Fig. 3.

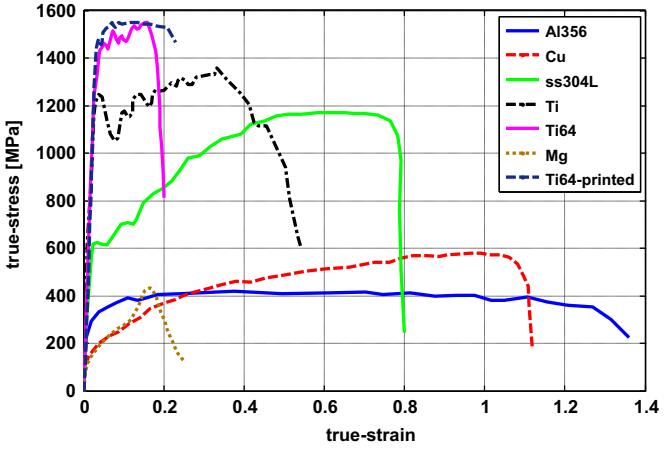

Fig. 3. Dynamic compression stress–strain curves obtained from Kolsky-bar (SHPB) tests. Strain rates are 3000–5000 s^{-1}.

3.1. Material characterization

3.1.1. Specimen processing

Each specimen was processed through the following stages:

Microstructural characterization – A metallographic specimen was prepared to characterize the initial microstructure and the average grain-size. Characterization was done for a non-tested machined specimen.

Sectioning – The specimen was (diamond/alumina) cut close to the mid section, to avoid edge effects. The uniform part of collapsed specimen was estimated to be at least 20 mm long.

Polishing – The sectioned specimen was embedded in an epoxy resin and polished using a semi automatic polishing machine following gradual the usual stages of coarse to fine grinding, using diamond fluids with 9 μm and 3 μm particles. Final (0.04 μm) polish was achieved using a colloidal silica suspension, which also causes initial specimen etching as well.

Etching – Specific etching reagents were used for each material: Kalling's #2 for SS304L, Kroll's solution for CP-Ti and Ti6Al4V, 10% NHO_3 for OFHC Cu. For the cast Mg-AM50 and Al-A356, the etching achieved from the colloidal solution was sufficient to reveal their microstructure.

Analysis – Optical microscopy (Nikon L-150) was used with a high-resolution camera. Full frame pictures of the specimen were obtained by stitching 10–12 pictures taken at a magnification of 100x.

3.1.2. Results of microstructural characterization

The polished and etched specimens reveal the multiple shear bands' pattern at different stages of collapse. For each specimen we characterized the following parameters:

- *Final dimensions* – We measured the dimensions of the collapsed cylinders with an optical microscope. These measurements determined the final effective strain reached in the experiment.
- *Number and length of shear bands* – Counting all shear bands of all lengths.
- *Shear band distribution* – We created a high-resolution picture and mapped the shear bands, resulting in the distribution of band lengths as a function of the polar position (as in Xue et al. (2004, 2002), Meyers et al. (2003)). For a *quantitative* description of shear band distribution, a probabilistic measure is needed, which highlights the statistical character of shear bands' occurence at each point in both directions of maximum shear stress, $\pm 45°$. After examining several probability functions, we adopted an empirical cumulative distribution function (ECDF) (Lovinger et al., 2011). The ECDF does not follow a particular parametric form of a probability function, but produces a non-parametric density estimate that adapts itself to the data. The stair-step function simply assigns a probabiliy of $1/n$ to each of *the n* observations in a sample. We use Greenwood's formula (Cox and Oakes, 1984) for calculating lower and upper confidence bounds for the calculated ECDF.
- *Average spacing between shear bands* – As will be further discussed, we found that the number of shear bands remained constant during the collapse process, thus, new shear bands do not initiate during the later stages. The significant value of spacing will be that at the initiation stage, referring to one of the basic questions of this research, namely what defines the spacing between shear bands for different materials.

As we examined specimens at different stages of collapse, the spacing between shear bands changed (became smaller) with the extent of collapse. Thus, we worked out a way to normalize the results. Clearly, the spacing should be obtained by

$$\text{Spacing} = \frac{2\pi R^*}{N_{SB}} \tag{6}$$

where $R*$ is the inner radius of the cylinder upon band initiation and N_{SB} is the total number of shear bands. The radius upon initiation is calculated through the definition of the equivalent failure strain:

$$\varepsilon_p^{eff} = \frac{2}{\sqrt{3}}\varepsilon_{rr} = \frac{2}{\sqrt{3}}\ln\frac{R^*}{R_0} = \varepsilon_f \tag{7}$$

where ε_f is the equivalent failure strain, ε_p^{eff} is the equivalent plastic strain, ε_{rr} is the radial strain, R_0 and $R*$ are the inner boundary radii at the initial stage and at shear band initiation, respectively. The failure strain at which initiation occurs is calculated from our calibrated failure criterion for shear band formation. We are using a strain energy density criterion which incorporates the physics of a *process* leading to shear band initiation and evolution rather than a threshold criterion like a value of strain. We define W as the strain energy density:

$$W = \frac{1}{\rho}\int_{\varepsilon_1}^{\varepsilon_2}\sigma d\varepsilon_p \tag{8}$$

where σ is the equivalent stress, ε_p is the effective plastic strain and ρ is the material density. We define a damage parameter $0 \le D \le 1$ evolving by

$$D = \frac{W - W_i}{W_f - W_i} \qquad W_i < W < W_f \tag{9}$$

where W_i is the strain energy density until the onset of shear initiation and W_f is the strain energy density at full localization when the flow stress in the band decreases to zero. D is used to decrease the flow stress, Y, through

$$Y = Y_0 \cdot (1 - D) = Y_0 \frac{W_f - W}{W_f - W_i} \tag{10}$$

where Y_0 is the initial flow stress of the material. We used this model in our numerical simulations and calibrated it for all of the materials we tested.. This model was used successfully also in the recent work of Dolinski et al. (2010) for reproducing shear bands in scenarios of forced shear localization.

We calculated the initial strain (ε_f) from the calibrated Wi parameter, integrating the stress–strain curves which appear in Fig. 3:

$$W_i = \frac{1}{\rho} \int_0^{\varepsilon_{cr}} \sigma d\varepsilon$$
$$Wi^* \rho = \int_0^{\varepsilon_f} \sigma d\varepsilon \Rightarrow \varepsilon_f \tag{11}$$

With the determined failure strain, we then calculate R^*, using Eq. (7) and then the spacing is determined using Eq. (6). However, as will be shown in the summary of the results (Table 3), the calculated spacing is not very sensitive to the exact value of the failure strain.

At this stage, we should note two remarks:

- The definition of the effective plastic strain in Eq. (7) is derived under simplified assumptions of material incompressibility to provide a simple measure for the average strain in the tests, as well as for comparison between different specimens. As pressures are not very high in the specimens (calculated by numerical simulations, not presented in the scope of this paper), the assumption of incompressibility is expected to be not very far from the actual value of the effective plastic strain. Yet, this definition of strain is different from the effective plastic strain calculated further in the numerical code, where compressible flow is taken into account.
- This definition of spacing is different from that used in the literature, e.g. Xue et al., (2004). In references Xue et al. (2004, 2002), Meyers et al. (2003), an extra factor of $\sqrt{2}$ multiplies Eq. (6), as a geometrical factor, referring to the 45 degree shear band direction of propagation. We found this factor to be superfluous at the initiation stage, when shear bands just initiate on the inner boundary (when the spacing is to be defined), and they are still radially oriented.

4. Experimental results

The experimental results are presented in this section for the seven materials tested in this work. A detailed analysis following the above explained characterization is presented in detail for one material, SS304L, while for the others, the results are given in a shortened version, mainly focusing on the measured spacing and number of shear bands and special observed additional features of relevance to this work.

4.1. Results for SS304L

The material was annealed, with an average grain size of ~100 μm and apparent twins, shown in Fig. 4. Dynamic strength was measured using the Kolsky-bar test (Fig. 3).

The results of two out of the seven tested specimens are shown in Fig. 5. On the polished specimens before etching, the inner copper cylinder and remains of the outer copper cylinder are evident. Joule heating of the outer copper cylinder causes melting of the external side of the cylinder, and in most of the specimens, only small melted remains are found on the collapsed specimen (see Fig. 5c). The current flows through the outer surface of the external Cu cylinder and the specimen is heated only by conduction from the external copper. As the overall time of collapse, calculated by simulations is about 8 μsec, the specimen is not significantly heated over this short duration, having a negligible effect on the formation of the shear bands.

The inner copper stopper was recovered with a hole at its center, as seen in Fig. 5a and c. After measuring the collapsed dimensions and calculating the materials' volumes we found that the copper came to a full collapse into the center, and the observed hole in the center was created by a hot jet which formed when the copper collapsed upon itself. Evidence of the copper jets was found also on a witness plate, placed perpendicular to the cylinders' axis and in Fig. 5a and c the solidified melted copper is evident around the hole.

Fig. 5b and d are the etched cross sections which reveal all of the shear bands in the specimens, while before etching (Fig. 5a and c), only shear bands which opened to cracks are evident. The average effective plastic strain of the specimens was calculated using Eq. (8). For each specimen, the number of shear bands at all lengths was counted. These are detailed in Table 1.

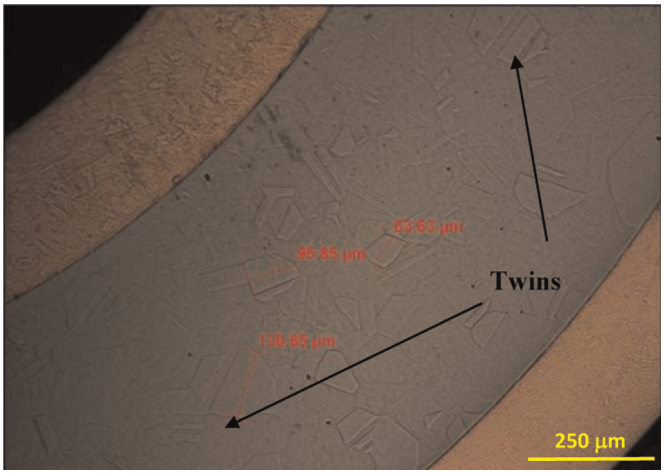

Fig. 4. SS304L: original microstructure.

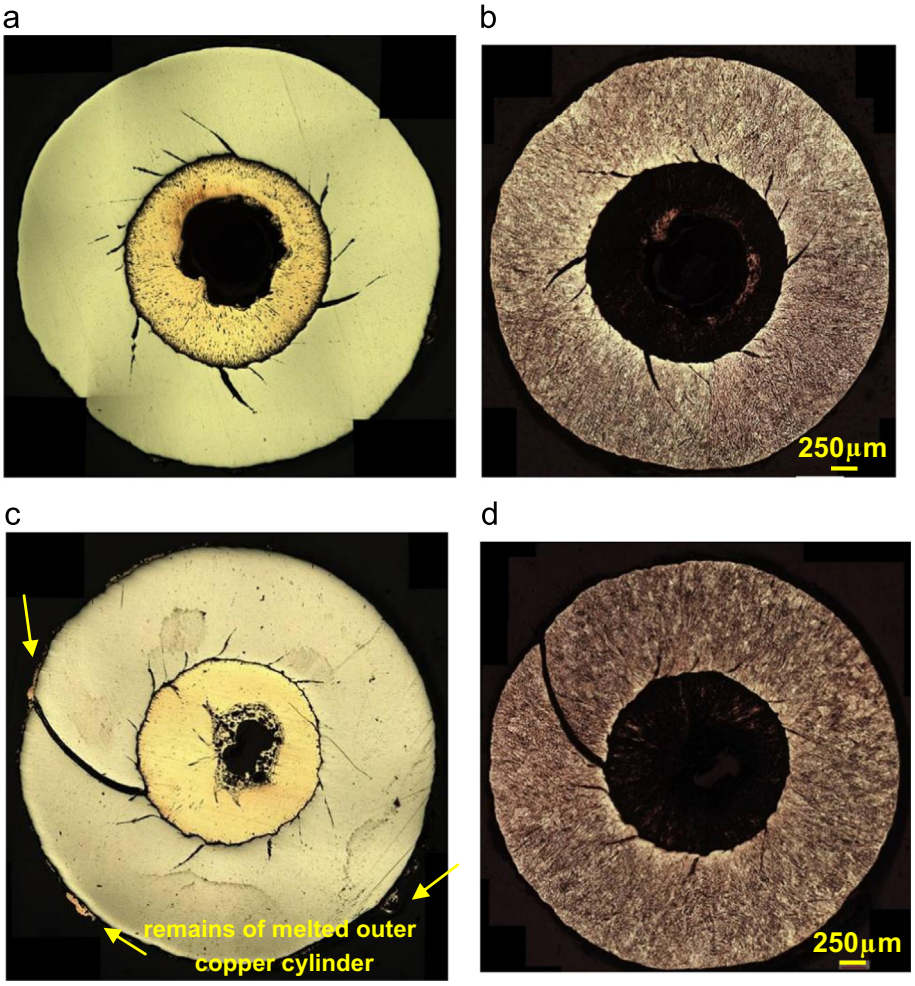

Fig. 5. Collapsed SS304L specimens: SS304L#1 ($\varepsilon_{Avg}=0.66$): (a) polished, (b) etched, SS304L#2 ($\varepsilon_{Avg}=0.80$): (c) polished, and (d) etched.

The number of shear bands in all of the specimens, at different stages of collapse, with average plastic strains of 0.37-0.80, is practically the same. This significant finding shows that the number of shear bands remains constant from the stage of initiation during all stages of collapse. The average number of shear bands in the SS304L specimens was $N_{SB}^{SS3_04L}=52$.

Table 1
Results for collapsed SS304L specimens.

Specimen number	D_0 – Initial inner diam [mm]	D_f – Final inner diam [mm]	Average effective plastic strain2/$\sqrt{3}\cdot\ln(D_0/D_f)$	Number of shear bands
1	3.5	1.98	0.66	52
2	3.5	1.76	0.80	52
3	3.5	2.34	0.46	52
4	3.5	2.33	0.47	53
5	3.5	2.53	0.37	51
6	3.5	2.44	0.42	52
7[a]	3.5	1.83–1.90	0.71–0.75	50–52

[a] Specimen #7 was examined at 3 different sections, thus the span of values.

The spacing is then calculated, referred to an average failure strain of 0.45 (calculated from the calibrated failure criterion we are using, as explained above). We calculate the radius at failure using Eq. (7), and then the spacing using Eq. (6):

$\text{Spacing}^{SS304L} = 0.143\text{mm} \pm 0.01\text{mm}$

We should point out that specimens #5 and #6, at an early stage of initiation, reach calculated average strains of 0.37 and 0.42, respectively, which are lower than the value we assigned to the failure strain (0.45). We explain this result by the difference between the average strain defined by a convenient approximation of an incompressible thin walled cylinder (Eq. (7)), and the in-situ strains which are highest at the inner boundary when calculating the strains in the in-fact thick-walled cylinder. For an *average* failure strain of 0.37, the strains at the inner boundary, where the shear bands initiate, already reach the calculated failure strain of 0.45. Moreover, we show later, in Table 3, that the calculated spacing is not very sensitive to the exact failure strain.

The distributions of the shear band lengths, for the two specimens are presented in Fig. 6. A shielding effect is noticed in the specimens: areas adjacent to the well developed shear bands are characterized by much shorter shear bands, since they develop within stress-relieved regions, where their propagation is slowed down or even completely arrested.

The ECDF for each of the specimens with the upper and lower confidence boundaries (UCB and LCB, respectively) are shown in Fig. 6e and f. The ECDF shows the typical distribution of shear band lengths in a collapsing cylinder: Many of the shear bands are small because they come to an early stop, due to the shielding effect. For both specimens one can see that about 70% of the shear bands have lengths smaller than 0.2 mm which are the "shielded" shear bands. In specimen SS304L#2, a single shear band, which propagated through the entire wall-thickness, is noticeable. We assume that this can occur in cases where a point disturbance, caused by the machining process, results in a stress concentration leading to a much earlier initiation of shear.

The ECDF is used to compare experimental results with simulations, or between different simulation results, as shown in Espinosa and Gailly (2001).

4.2. Results for pure titanium

The material was annealed. The original microstructure before deformation had an average grain size of $\sim$150 μm, with no twins apparent.

The results of two specimens after etching are shown in Fig. 7. A smaller number of shear bands was found in these specimens in comparison with the SS304L specimens.

The average number of shear bands in the CP-Ti specimens was $N_{SB}^{Ti} = 31.5$.

The spacing is calculated, referring to a failure strain of 0.50:

$\text{Spacing}^{Ti} = 0.205\text{ mm} \pm 0.01\text{ mm}$.

Profuse twinning was observed, as shown in Fig. 8.

4.3. Opening of cracks in the evolved shear bands

An interesting result in the pure Titanium specimens relates to the mechanism of crack opening on evolved shear bands. We found clear evidence that the opening of cracks occurs through a mechanism of growth and coalescence of voids. In Fig. 9, a very fine, recrystallized structure is evident in the shear band, inside which one observes elongated voids which are close to each other. This observation corresponds to pore opening within the SB, where the material experiences high temperatures and very low strength (close to melting). Under these conditions, and reverberations of weak tension waves (rarefaction waves emanating from the free boundaries), pores can open and eventually coalesce to a continuous crack, as seen in Fig. 9b. The shape of the elongated voids indicates that they grow under shear stresses. This phenomenon was reported in several works in the literature for Titanium, Ti6Al4V, steel 4340 and U-2Mo (Giovanola, 1988a, 1988b; Grebe et al., 1985; Me-Bar and Shechtman, 1983; Rogers, 1979; Dodd and Atkins, 1983), including numerical simulations by Teng et al. (2007). This phenomenon was not observed in the other materials which we studied, and it certainly needs further investigation.

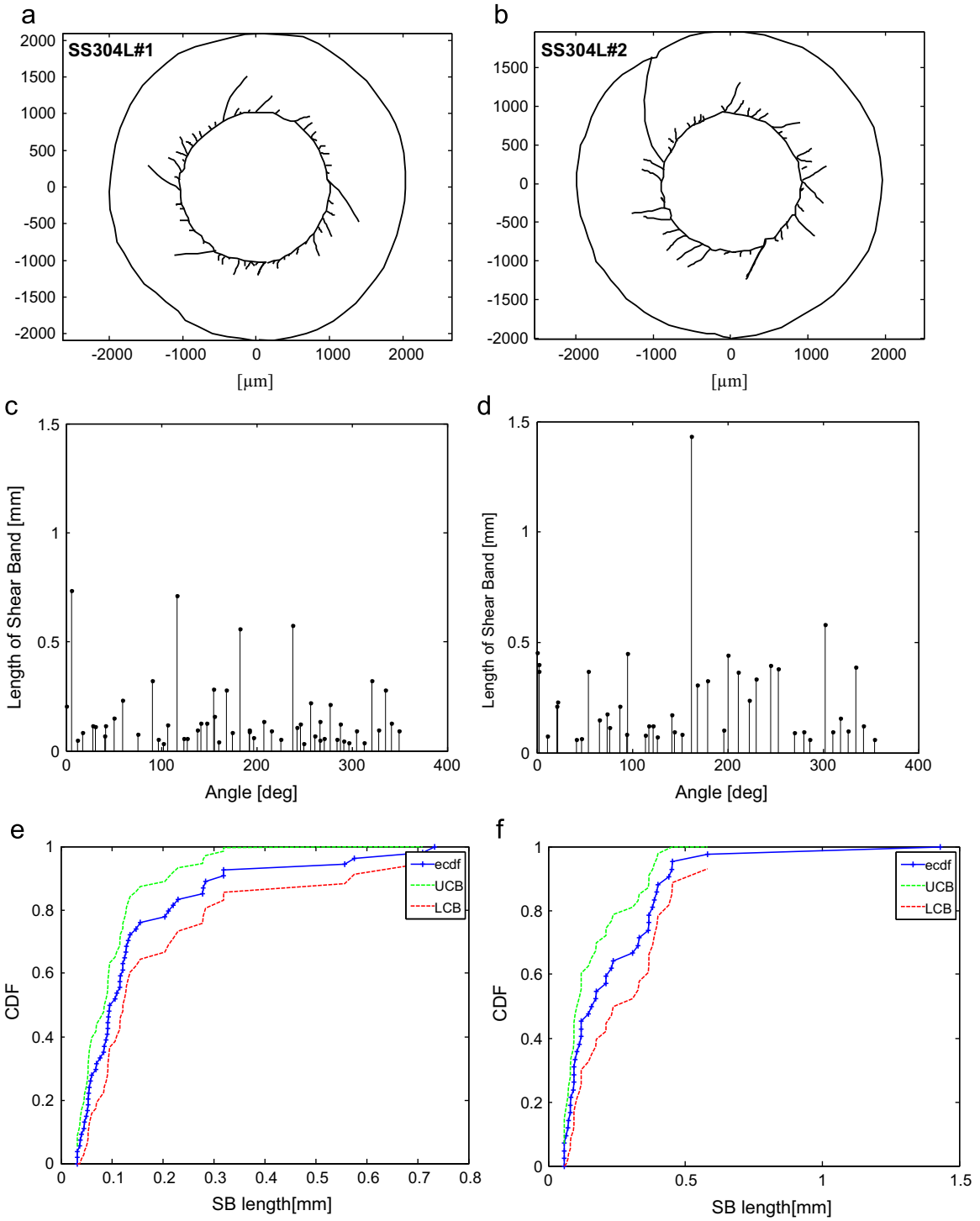

Fig. 6. Shear band distribution in specimen SS304L#1, SS304L#2 (a) and (b) specimen sketch using image procedure; (c) and (d) SB length distribution; (e) and (f) calculated ECDF (UCB and LCB are the upper and lower confidence boundaries).

4.4. Results for wrought Ti6Al4V

We used an annealed material, for which the original microstructure before deformation had an average grain size of ~1–2 μm. The results of three specimens, after etching are shown in Fig. 10. The shear bands in Ti6Al4V apparently occur at a very early stage, as expected from the stress–strain curves of Ti6Al4V in the Kolsky-bar tests. In order to reach the stage of

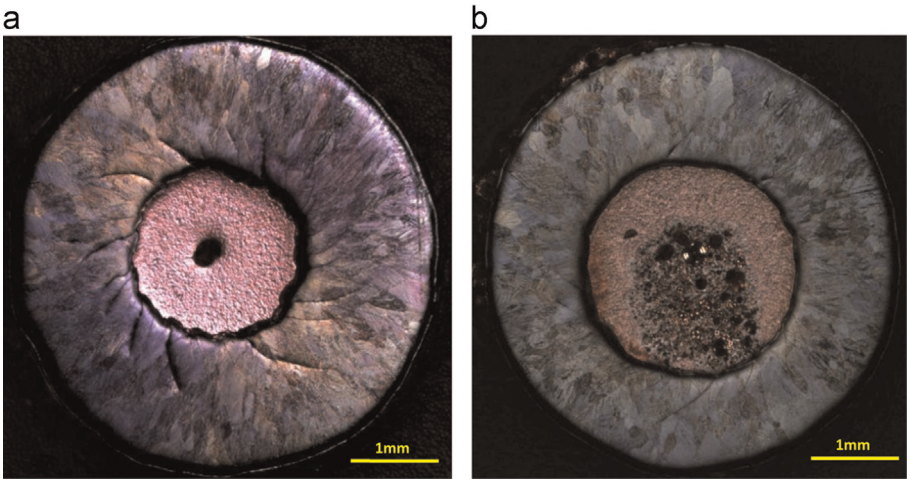

Fig. 7. Collapsed titanium specimens (after etch): (a) Ti#1 ($\varepsilon_{Avg}=0.85$) and (b) Ti#2 ($\varepsilon_{Avg}=0.46$).

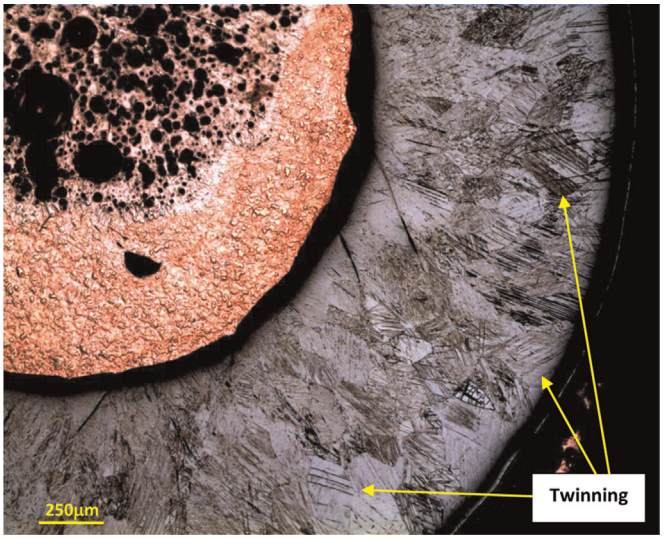

Fig. 8. Extensive twinning is collapsed titanium specimen Ti#1.

band initiation, only a minor collapse is needed, with relatively low magnetic pressures. The inner copper cylinder at this stage did not fully collapse and was found separated from the specimen. At higher driving pressures, the shear bands which evolve at an early stage, traverse the specimen's thickness dimension, separating the cylinder into fragments. These collapse on onto the other, without experiencing additional plastic strains.

The calculated average plastic strain of specimen Ti6Al4V#2 (Eq. (7)) was 0.23. For the sheared-through specimens, the average effective plastic strain could not be defined as the final geometry is a result of the rigid body motions of the fragments.

The average number of shear bands in the wrought Ti6Al4V specimens was $N_{SB}^{Ti6Al4V}=20$. The spacing is then calculated, referred to a failure strain of 0.2:

$\text{Spacing}^{Ti6Al4V}=0.46\text{ mm}\pm 0.02\text{ mm}$.

The number of shear bands in Ti6Al4V was much lower than in all the other materials. The combination of an early initiation stage with the small number of shear bands results in a large spacing, in comparison with CP-Ti or SS304L.

4.5. Results for LMD-fabricated Ti6Al4V

The Ti6Al4V produced by Laser Metal Deposition (LMD) was chosen to examine the effect of the microstructure on the initiation of shear bands. This technology “prints” the material in layers of 30 μm: A layer of Ti6Al4V powder is placed on a

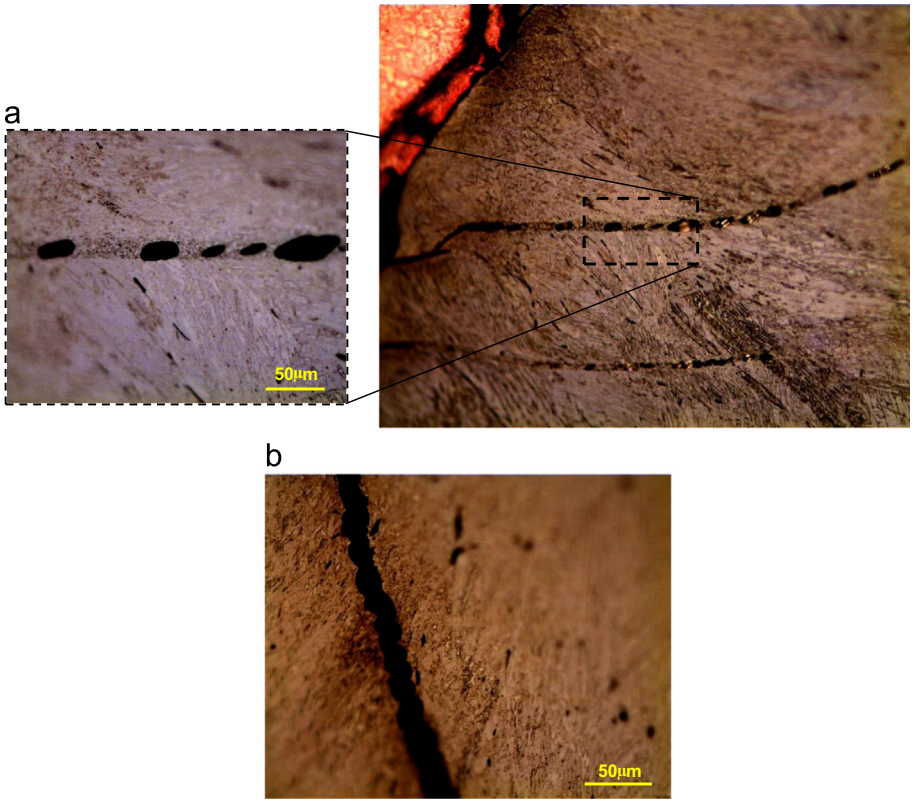

Fig. 9. Crack opening within shear bands through void growth and coalescence: (a) void growth in a shear band and (b) a continuous crack as a result as void coalescence.

working plane and then melted by the heat of a laser which tracks the pre-programmed geometry of the prescribed layer. For our specimens we manufactured rods of 10 mm in diameter, which were machined into cylindrical specimens. After the LMD process, the rods were heat treated for 4 h at 700 C°.

The microstructure had an average grain size of ~100 μm, which is much larger than the 1–2 μm grain size of the wrought material. The dynamic stress–strain curve, measured by the Kolsky-bar configuration (Fig. 3), showed two main differences in comparison with that measured for the wrought material: (1) a slightly higher strength of about 5%, and (2) the absence of strain hardening. On the other hand, no significant change in the failure-strain was measured (about 0.2 for both materials).

Pictures of etched specimens Ti6Al4V-LMD#1 and Ti6Al4V-LMD#2 are shown in Fig. 11. Similar results were also obtained in the wrought material at different extents of the collapse. We managed to conduct the weak collapse experiment (specimen #1) at an even earlier stage with average strain of only 0.1.

The average number of shear bands in the Ti6Al4V-LMD specimens was $N_{SB}^{\text{Ti6Al4V-LMD}}=21$.The spacing is calculated, with a failure strain of 0.2, resulting in

$\text{Spacing}^{\textbf{Ti6Al4V-LMD}}=0.43\ \text{mm}\pm 0.02\ \text{mm}$

As discussed above, the difference between the average and local strain explains the difference between the definition of the average value of the plastic strain (0.1), defined for the Ti6Al4V-LMD#1 specimen, and the 0.2 failure strain we used to calculate shear band initiation at the inner boundary. The shear band evolution in the Ti6Al4V-LMD specimens was found to be similar, at the low and high plastic strains, to that of the wrought material despite the significant differences in microstructure and grain size. We further compared the shear band patterns to the results obtained for hot isostatically pressed (HIPed) Ti6Al4V by Gu and Nesterenko (2007). The collapsed TWC of the HIPed material demonstrated a different behavior, with a better volume distributed deformation pattern, what seems as a more ductile behavior. We believe this to be a result of different micro deformation mechanism in the HIPed material, also indicated by the additional differences in the shear band patterns such as multiple bifurcations of the major shear bands, which were not evident in any of materials we examined.

4.6. *Results for Mg-AM50*

The Mg-AM50 alloy was expected to behave in a similar manner to the Ti6Al4V alloy, with a small initiation strain and a large spacing between shear bands. This assumption was based on the fact that in the Kolsky-bar tests (Rittel and Wang, 2008), both materials fail at low strains of 0.17–0.25.

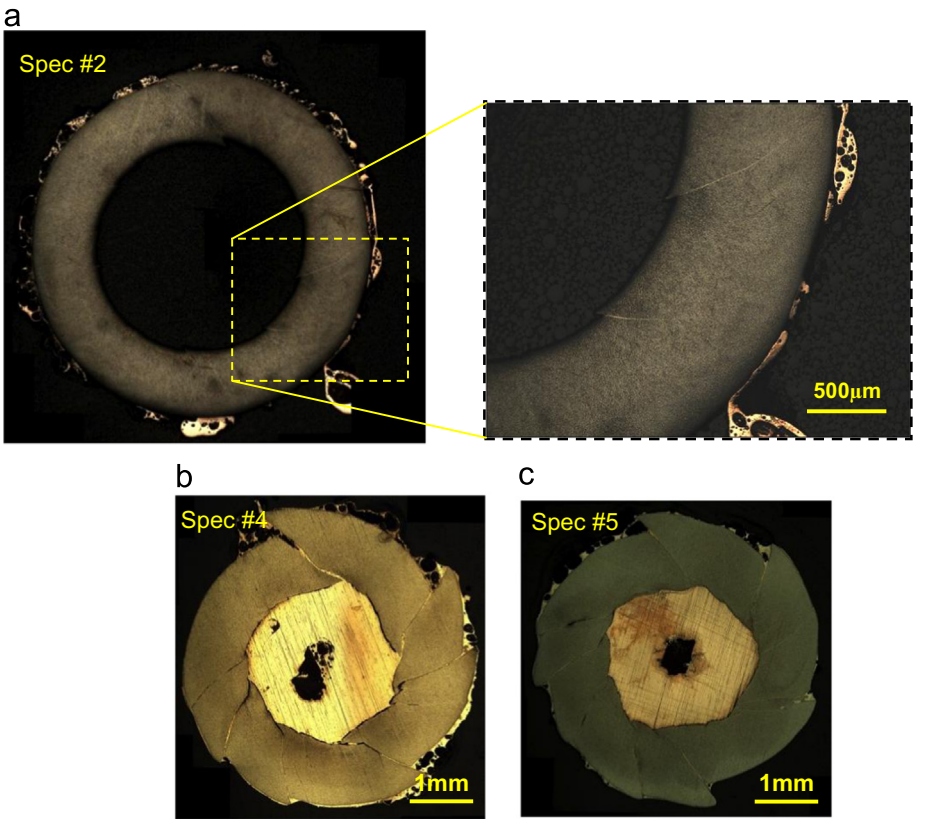

Fig. 10. Collapsed wrought Ti6Al4V specimens (after etch): (a) Ti6Al4V#2 ($\varepsilon_{Avg}=0.23$); (b) Ti6Al4V#4; and (c) Ti6Al4V#5.

The magnesium alloy Mg-AM50 is a cast material with 95% Mg, ~5% Aluminum and small quantities of Mn and Zn. The original microstructure before deformation had an average grain size of ~10 μm.

Pictures of specimens MgAM50#1 and MgAM50#2, with corresponding average effective plastic strains of 0.31 and 0.42, are shown in Fig. 12. Surprisingly, the behavior was very different than that of Ti6Al4V, and closer to a more "ductile" behavior such as that of the CP-Ti: A large number of shear bands evolved with a relatively homogeneous distribution, and no shear bands reached the external boundary of the specimen.

The average number of shear bands in the Mg-AM50 specimens was $N_{SB}^{Mg}=35$.The spacing is calculated, with a failure strain of 0.3. This failure strain, calculated from the energy failure criterion, was larger than what has been reported for this material in Kolsky-bar tests (~0.2, Rittel and Wang, 2008). We believe the higher failure strain in the TWC tests is due to the pressure dependence of the failure strain in Magnesium, as reported in Hanina et al. (2007). The calculated spacing for Mg-AM50 was: $\text{Spacing}^{Mg}=0.24\text{ mm}\pm0.01\text{ mm}$.

4.7. Results for Al-A356

Aluminum Al356 is a sand-cast aluminum alloy with 90% Aluminum and 7% Silicon with small quantities of Fe, Cu, Ti and Zn. The Al-A356 is rather brittle in tension (failure strain of 0.035), but was found to be very ductile under compression in the Kosky bar tests (Fig. 3). Clearly, this material did not fail even compressed to plastic strains of ~1.2.We used a sand-cast aluminum with a T6 heat treatment.

We conducted a single test on this material, finding only 2 shear bands initiating at 0.7 average plastic strain reached in the test (Fig. 13). The silicon phase, shown as gray needles, is aligned along the trace of plastic flow and a significant radial alignment is noticeable. Basically, no shear bands evolved for this material up to the average strain of 0.7.

4.8. OFHC copper

OFHC copper specimens were used in order to examine grain size effect on the shear band distribution. As explained in the introduction, the two materials for which grain size effect was examined so far were SS304L (Xue et al., 2004) and OFHC copper (Bondar and Merzhievskii, 2006). We chose to examine OFHC copper in our research for the following reasons:

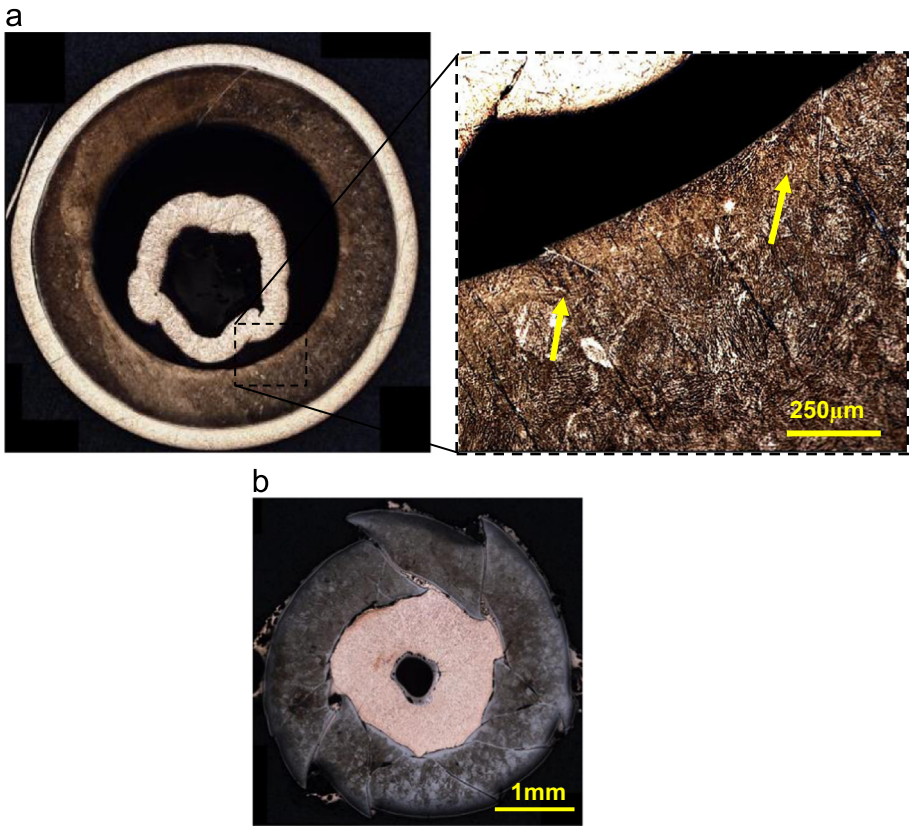

Fig. 11. Collapsed Ti6Al4V-LMD specimens (after etch): (a) Ti6Al4V-LMD#1 (ε_{Avg}=0.10) and (b) Ti6Al4V-LMD#2.

(1) Copper was reported in Bondar and Merzhievskii (2006) to have a significant grain size effect on the formation of ASBs, even at relatively low strains.
(2) Copper has a very small Hall–Petch effect (Bondar and Merzhievskii, 2006). The work done on SS304L (Grady and Kipp, 1987) showed no grain size effect, but had a significant Hall–Petch effect resulting in differences in the yield strength, which may have a "balancing" effect when combined with the change of grain size. Copper, on the other hand, has a negligible Hall–Petch effect, which enables a more unequivocal assessment of the grain size effect, if any.

The original material was a 50 mm diameter rod with an initial grain size of 150 μm. We used ECAP (Equal channel angular pressing) to breakdown the material grain size to an average size of 20 μm. The ECAP'ed rods were then wire-cut to 9 mm diameter rods. The small rods were heat treated in order to obtain different grain sizes and then machined to the cylindrical specimens' final dimensions.

Different grain sizes were obtained by applying the following heat treatments:

	Heat treatment	Average grain-size
Cu-I	500 C°@6 h	20 μm
Cu-II	600 C°@3 h	100 μm
Cu-III	800 C°@1 h	200 μm
Cu-IV	900 C°@1/2 h	300 μm

The influence of grain size on shear band initiation was examined in Bondar and Merzhievskii (2006) for "small grain" (~30–50 μm) and "large grain" (150–200 μm) copper. A pronounced difference between the two materials was observed: the small grain copper showed no shear bands whereas the large grain copper did, at a relatively low plastic strain of 0.26. The four classes of grain-size obtained in our work were meant to widen the span of grain size in order to refine and better understand the results and conclusions in Bondar and Merzhievskii (2006).

We conducted Kosky-bar tests to compare the dynamic strength of the different coppers, presented in Fig. 14. The results show very similar stress strain curves for all specimens (the differences are within the experimental errors), confirming a lack of significant Hall–Petch effect for the selected grain sizes.

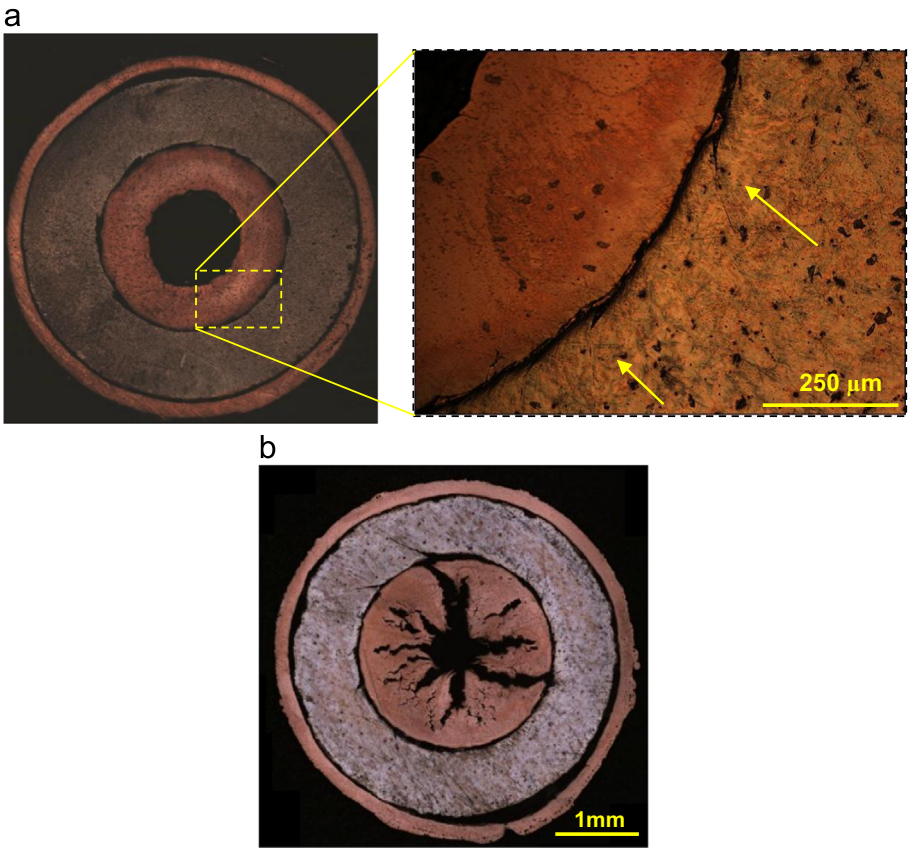

Fig. 12. Collapsed Mg-AM50 specimens (after etch): (a) MgAM50#1 (ε_{Avg}=0.31) and (b) MgAM50#2 (ε_{Avg}=0.42).

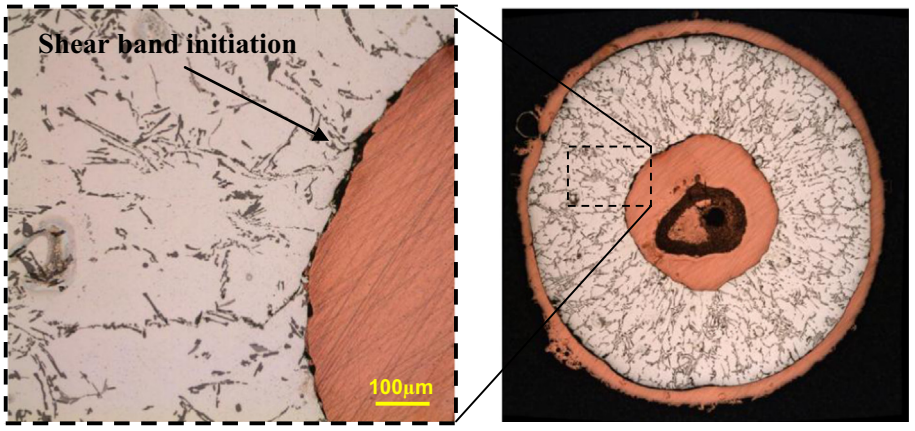

Fig. 13. Collapsed Al-A356 specimen Al-A356#1.

Pictures of collapsed copper specimens with different grain sizes, after etching, are shown in Fig. 15. The geometrical properties of the different specimens we examined are presented in Table 2.

No shear bands were found in all of the specimens. Since this result contradicts reported results in the literature, we further examined the copper specimens using SEM (scanning electron microscopy). We identified 3–4 faint shear band initiations in each of the specimens, about 10 μm long (see Fig. 16). These initiations were mostly grouped at one site and did not show a collective behavior as seen in other materials, thus we did not consider this finding as a definite evidence for shear banding, rather, it is a local behavior, due to a local machining flaw.

A recrystallized layer (100–150 μm) was evident at the inner boundary of the collapsed specimen (Fig. 16). This layer was ruled out to be a result only from the machining of the specimen, as its thickness was measured on the initial geometry to be much smaller, about 20 μm.

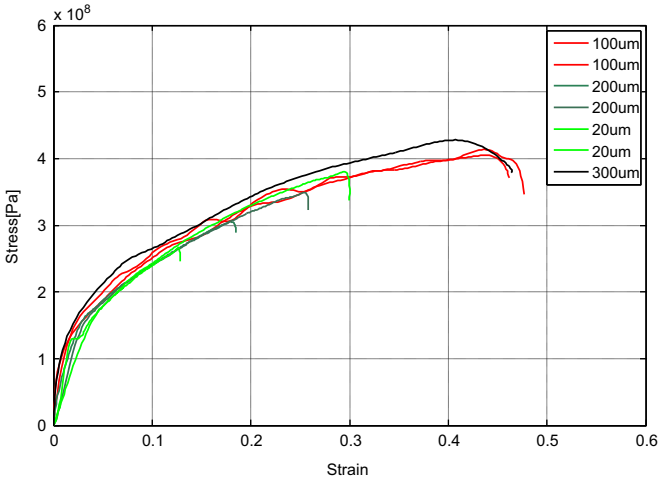

Fig. 14. Stress strain curves for copper with different grain sizes (strain rate ~3000–4000 [1/s]).

Profuse twinning is evident at the inner boundary, following the recrystallized layer. It can be surmised that the recrystallized layer and intense twinning might be joint mechanisms holding back the shear localization, as will be discussed later.

For the coarse grain sizes of 200 μm and 300;μm, the inner boundary of the specimen is distorted due to the limited deformation/rotation of the large grains (like the "orange peel" surface texture in tension tests of coarse grained materials (Rittel et al., 1991)).

4.9. Summary of the results

The measured number of shear bands and spacing for all tested materials are summarized in Table 3. The spacing was estimated by using the compression failure strain, as calculated from the energy criterion, presented above. Nevertheless, we include a large span of ± 0.05 as an error bar, which in turn induces a very small change in the spacing values of ± 0.01 mm for most materials, and ± 0.02 mm for the Ti6Al4V spacing.

5. Discussion

From the above experimental results, two main issues can now be addressed, namely:

(1) How do the present results compare with those of the larger specimens tested in the explosively driven thick wall cylinder (ED-TWC) experiments, which were reported in Xue et al. (2004, 2002), Meyers et al. (2003).
(2) How do the present results compare with the theoretical approaches predicting the shear band spacing for different materials.

5.1. Comparison with ED-TWC experiment

The geometry of the specimens tested in this research is scaled down by a factor of 4 in comparison with the geometry tested in the explosively driven experiments of Xue et al. (2004, 2002), Meyers et al. (2003). Also, as noted above, we defined the spacing differently than in those references, so for comparison we calculated the spacing in the ED-TWC specimens using our definition, namely dividing the corresponding radii upon initiation by the number of shear bands. This way, we can compare our results for SS304L, CP-Ti and Ti6Al4V, as summarized in Table 4.

As is clearly seen, our results are in good agreement with those of Xue et al. (2004, 2002), Meyers et al. (2003), with differences of only 10–20%, despite the large scale-factor of the specimens.

The slightly larger spacing in the explosively driven tests could be possibly explained by the smaller strain rate in ED tests, as compared to EM experiments ($\sim 6\text{-}8 \cdot 10^4\ s^{-1}$ vs. $\sim 2\text{–}3 \cdot 10^5\ s^{-1}$, respectively).

It can be concluded from this comparison that the spacing between shear bands does not depend on geometrical dimensions of the specimen (e.g. radius, wall thickness) but rather on material properties.

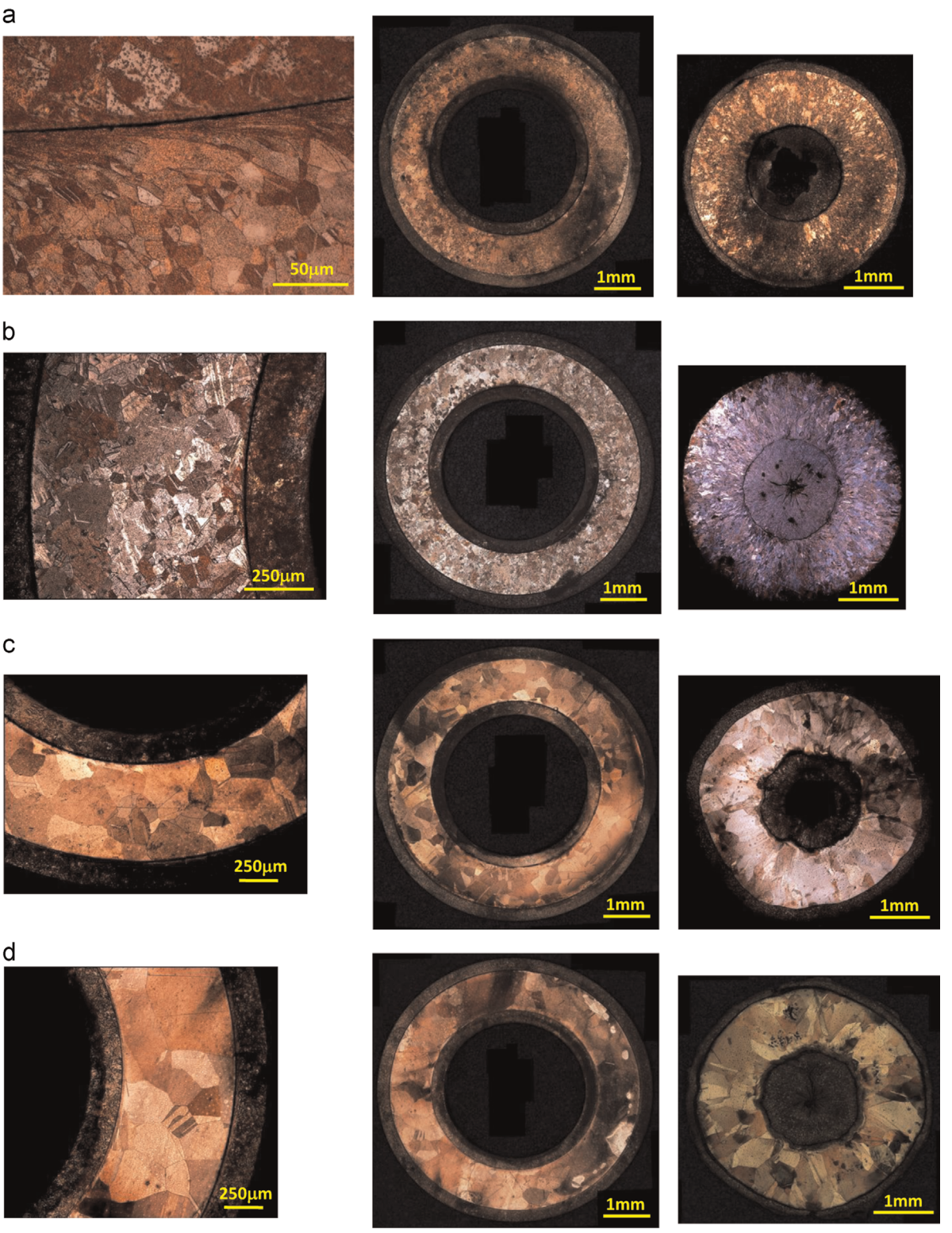

Fig. 15. Copper specimens before and after collapse: (a) 20 um; (b) 100 um; -/ti–> (c) 200 um; and (d) 300 um.

Table 2
Results of collapsed copper specimens.

	D_0 – Initial inner diam [mm]	D_f – Final inner diam [mm]	Effective plastic strain2/ $\sqrt{3}\cdot \ln(D_0/D_f)$	Number of shear bands
Cu_I_1	**3.3**	**1.95**	**0.61**	–
Cu_I_2	**3.3**	**1.58**	**0.85**	–
Cu_II_1	**3.3**	**1.77**	**0.72**	–
Cu_III_1	**3.3**	**1.83**	**0.68**	–
Cu_III_2	**3.3**	**1.58**	**0.85**	–
Cu_IV_1	**3.3**	**1.81**	**0.70**	–

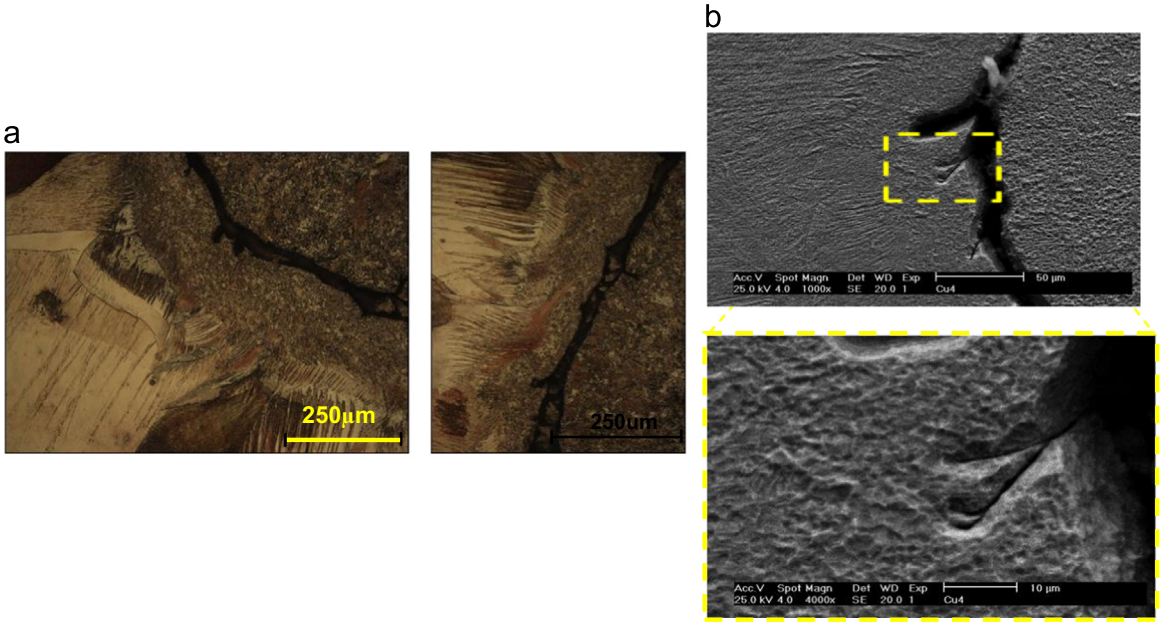

Fig. 16. Microstructure examination in specimen Cu-IV-1: (a) profuse twinning and recrystallized inner layer and (b) SEM figure showing one of three eventual faint shear band initiations.

Table 3
Results summary for all tested materials.

Material	Grain size [μm]	Average number of shear bands	Compression failure strain	Spacing [mm]
CP-Ti	150	**32**	0.50 (0.45–0.55)	**0.205** (0.2–0.22)
Ti6Al4V wrought	2	**20**	0.20 (0.15–0.25)	**0.46** (0.44–0.48)
Ti6Al4V LMD	100	**21**	0.20 (0.15–0.25)	**0.43** (0.42–0.46)
ss304L	100	**52**	0.45 (0.40–0.50)	**0.14** (0.13–0.15)
Mg-AM50	10	**35**	0.30 (0.25–0.35)	**0.24** (0.23–0.25)
Al-A356	100	No SB	> 0.70	–
Cu-I	20	No SB	> 0.85	–
Cu-II	100	No SB	> 0. 85	–
Cu-III	200	No SB	> 0. 85	–
Cu-IV	300	No SB	> 0. 85	–

5.2. Comparison with theoretical spacing models

As mentioned earlier, the three main models for spacing are those of Wright and Okendon (1996), Molinari (1997) and Grady and Kipp (1987). The published experimental results in the literature are compared with these models, and we examine here their ability to predict the spacing between shear bands for a wide variety of materials. The models of Wright

Table 4
Comparison of shear bands' spacing between the EM and explosively driven TWC tests.

Material	Electro-magnetically driven TWC-tests (this work) [mm][a]	Explosively-driven TWC tests [mm][a]
Ti	0.20–0.22	0.24–0.25
Ti6Al4V	0.44–0.48	0.53–0.58
SS304L	0.13–0.15	0.11–0.17[b]

[a] Spacing evaluation was calculated with the range of failure strains given in Table 3.
[b] For the ED SS304L specimens the number of shear bands had a large span (192–272), thus the large range of spacing.

and Ockendon and of Molinari refer to the initiation stage, thus we can compare our results to their predictions. However, since the model of Grady and Kipp aconsiders well developed shear bands, it is of a lesser relevance here. The expressions derived by Wright and Okendon (1996) and Molinari (1997) are shown in Eqs. (2) and (4).

The data used for our calculations are listed in Table 5, and the calculated spacings are given in Table 6. The strain rates in our tests were taken from the numerical simulations, and we used here an average value of $\dot{\gamma}=2\cdot 10^5\ s^{-1}$.

From the comparison between the calculated and the experimental spacings, one can draw the following conclusions:

(1) The theoretical expressions do not match the experimental results, as far as the spacings are considered.
(2) The high strain rate in our tests has a pronounced effect on the calculated spacing values. While for the explosively driven tests, the spacing values for CP-Ti and SS304L Xue et al. (2004, 2002), Meyers et al. (2003) showed a limited match with the models, the current higher strain rate (by a factor of 5) results in much smaller spacing values, for which the matching is lost. The strain rate effect seems to override all other differences in the coefficients, according to a variety of values reported in the literature.
(3) The models predict small differences in the spacing of CP-Ti and Ti6Al4V, as found also in the work of Xue et al. (2004). Yet, our experimental results show a factor of 2–3 between the two materials.
(4) The models predict spacing values for aluminum and copper, which do not agree with our experimental results, in which shear bands did not evolve.

At this stage, the observed discrepancy between theoretical predictions and measured spacing values can be tentatively attributed to two reasons:

(1) The first reason is that the analytical models lack an accurate physical input of the mechanisms driving the formation of shear bands.
(2) One possibility can be that the assumed dominance of thermal softening effects for shear band initiation, as the basis of these models, should be modified to include other physical causes for material softening, as suggested in Osovski et al. (2012), Rittel et al. (2008).

It should be noted that in recent publications examining the collapse of thick walled Ni-Al laminated cylinders (Chiu et al., 2013; Olney et al., 2014, 2015), self-organized patterns of localized deformation were demonstrated, with no relation to shear band evolution. The mesostructure of the Ni–Al laminated cylinders had a significant influence on the mechanism of instability. Examining this result points out the mesostructure of the material as an additional factor aside than material properties to be considered, when searching how to explain the number of shear bands and their spacing in collapsing thick walled cylinders.

Table 5
Material properties for spacing calculation by Eqs. (2)–(5).

	Static shear strength, τ_0 [MPa]	Heat conduction, k [J/s m K°]	Heat capacity, c [J/kg K^0]	Thermal expansion coeff., a [K^0]$^{-1}$	Strain rate hardening coeff., m [–]
CP-Ti	300	20	530	6.2e−4	0.012
SS304L	300	16.2	500	4.5e−4	0.05
Ti6Al4V	400	5.8	530	6.2e−4	0.035
Cu	100	400	383	3.8e−4	0.025
Mg-AM50	125	100	1020	5.1e−4	0.025
Al-A356	150	200	900	6.2e−4	0.015

Table 6
Spacing calculation by Eqs. (2) and (4).

Material	Model	Calculated [mm]	Measured [mm]
CP-Ti	WO Molinari	0.075 0.07	0.205
Ti6Al4V (Wrought)	WO Molinari	0.11 0.10	0.46
Ti6Al4V (LMD)	WO Molinari	0.11 0.10	0.43
ss304L	WO Molinari	0.24 0.22	0.14
Mg-AM50	WO Molinari	0.31 0.29	0.24
Al-A356	WO Molinari	0.21 0.19	– (> 0.70)
OFHC- Cu	WO Molinari	0.42 0.39	– (> 0.85)

5.3. *Grain-size effect*

One of the goals of this research was to examine the influence of grain size on shear band initiation. The present results clearly show that the grain size has no effect on shear band initiation, and that grain boundaries do not play a significant role as initiation sites. This claim is supported by the following results:

(1) For OFHC-Cu specimens with various grain sizes (20–300 μm), we found only faint signs of SB initiation, irrespective of the grain size. This result is in contrast with the work of Bondar and Merzhievskii (2006), although the evidence of shear bands in this work is questionable.
(2) We examined Ti6Al4V with two radically different microstructures.Yet, the measured spacings between shear bands were practically the same for the two materials.
(3) Finally, for both CP-Ti and Ti6Al4V specimens, evidence of transgranular shear bands was found (Fig. 17).

6. Summary and conclusions

This work represents the first large scale study on spontaneous nucleation of adiabatic shear bands in various materials, to the best of the authors' knowledge. The outcome of this study is the generation of several physical observations that can serve as a basis for future analytical models on this shear instability mechanism. We would like to emphasize the following points. First, the shear band spacing is not characterized by a geometrical scale of the specimen size (e.g radius, wall

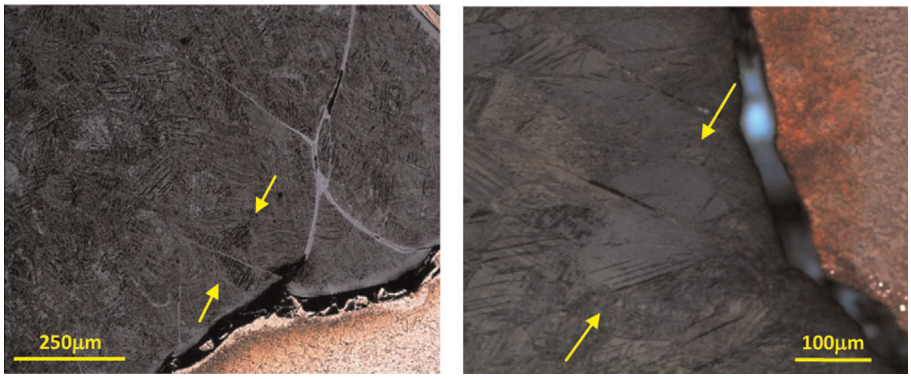

Fig. 17. Grain crossing evolution of shear bands in (a) Ti6Al4V-LMD#1 and (b) CP-Ti #1 specimens.

thickness) but rather by material properties. This confirms the character of spontaneous adiabatic shearing as a material rather than structural instability, when the two are generally hard to differentiate.

The next point is that the shear band spacing is not related to or dictated by the microstructure of the material (e.g. grain size). This observation strengthens a continuum type of approach for modeling, in which subtle microstructural details need not be taken into account, at least for engineering predictions.

Finally, the present study offers a wide experimental database which allows comparison with analytical expressions describing the shear band spacing. We showed that the analytical models examined here, do not adequately predict the measured spacings. The strong influence of the material's strain-rate sensitivity, which is outlined as a dominant factor in the theoretical predictions, was not found in the experimental data of the explosively and EM driven tests. It was suggested that the limited ability of the theoretical 1D models (W&O, Molinari) to predict spacing in the experiments seems to strengthen the notion that thermal softening is not the dominant factor responsible for the onset of localization. This point is currently examined through numerical simulations indicating micro deformation mechanisms are a dominant factor controlling the multiple shear band patterns.

Acknowledgements

We would like to acknowledge Dr. A. Rikanati, Mr. I. Gisis, Mr. U. Avni and Mr. E. Yeger for their assistance in conducting the experiments, and Mr. S. Aricha on designing the specimens. The financial support of the Israel Science Foundation – ISF (Grants 2017688 and 2109912) and of the Pazi Foundation are kindly acknowledged.

References

Bai, Y., Dodd, B., 1992. In: Adiabatic Shear Localization: Occurrence, Theories and ApplicationsPergamon Press, Oxford.
Bondar, M.P., Merzhievskii, L.A., 2006. Evolution of the metal microstructure and conditions of strain localization under high-strain-rate loading. Combust. Explos. Shock Waves 42 (3), 356–365.
Chen, Y.J., Meyers, M.A., Nesterenko, V.F., 1999. Spontaneous and forced shear localization in high strain-rate deformation of tantalum,. Mater. Sci. Eng. A 286, 70–82.
Chiu, P.H., Olney, K.L., Higgins, A., Serge, M., Benson, D.J., Nesterenko, V.F., 2013. The mechanism of instability and localized reaction in the explosively driven collapse of thick walled Ni–Al laminate cylinders. Appl. Phys. Lett. 102.
Cox, D.R., Oakes, D., 1984. In: Analysis of Survival DataChapman & Hall, London.
Davidenkov, N., Mirolubov, I., 1935. Tech. Phys. USSR 2, 281.
Dodd, B., Atkins, A.G., 1983. Flow localizationin shear deformationof void containing and void free solids. Acta Metall. 3.
Dabboussi, W., Nemes, J.A., 2005. Modeling of ductile fracture using the dynamic punch tests. Int. J. Mech. Sci. 47, 1282–1299.
Dodd, B., Walley, S.M., Yang, R., Nesterenko, V.F., 2015. Major steps in the discovery of adiabatic shear bands. Met. Trans. A 46 (2).
Dolinski, M., Rittel, D., Dorogoy, A., 2010. Modeling adiabatic shear failure from energy considerations. J. Mech. Phys. Solids 58, 1759–1775.
Dorogoy, A., Rittel, D., 2005a. Numerical validation of the Shear Compression Specimen (SCS). Part I: quasi-static large strain testing. Exp. Mech. 45 (2), 167–177.
Dorogoy, A., Rittel, D., 2005b. Numerical validation of the Shear Compression Specimen (SCS). Part II: dynamic large strain testing. Exp. Mech. 45 (2), 178–185.
Espinosa, H.D., Gailly, B.A., 2001. Modeling of shear instabilities observed in cylinder collapse experiments performed on ceramic powders. Acta Mater. 49, 4135–4147.
Grady, D.E., 1982. Local inertial effects in dynamic fragmentation. J. Appl. Phys. 53 (1), 322–325.
Grady, D.E., Kipp, M.E., 1987. The growth of unstable thermoplastic shear with application to steady-wave shock compression in solids. J. Mech. Phys. Solids 35 (1), 95–118.
Gu, Ya Bei, Nesterenko, V.F., 2007. Dynamic behavior of HIPed Ti–6Al–4V. Int J. Imp. Eng. 34, 771–783.
Grebe, H.A., Pak, H., Meyers, M.A, 1985. Adiabatic shear localization in titanium and Ti–6pct Al–4 pct V Alloy. Met. Trans. A 16.
Giovanola, J.H., 1988a. Adiabatic shear banding under pure shear loading – Part I – direct observation of strain localization and energy dissipation measurements. Mech. Mater. 7.
Giovanola, J.H., 1988b. Adiabatic shear banding under pure shear loading – Part II – fractographic and metallographic obsevrations. Mech. Mater. 7.
Hanina, E., Rittel, D., Rosenberg, Z., 2007. Pressure sensitivity of adiabatic shear banding in metals. Appl. Phys. Lett. 90.
Kalthoff, J.F., Wrinkler, S., 1987. Failure mode transition at high rates of shear loading. In: Chiem, C.Y., Kunze, H.-D., Meyer, L.W. (Eds.), Impact Loading and Dynamic Behavior of Materials, vol. 1; 1987, pp. 185–195.
Kravz-Tarnavskii, V.P., 1928. J. Russ. Metall. Soc. 3, 162.
Lovinger, Z., Rikanati, A., Rosenberg, Z., Rittel, D., 2011. Electro-magnetic collapse of thick walled cylinders to investigate spontaneous shear localization. Int. J. Impact Eng. 38, 918–929.
Lovinger, Z., Partom, Y., 2009. Simulation of multiple shear bands in collapsing cylinder experiments. In: Proceedings of the 8th International Conference on Mehanical and Physical Behaviour of Materials under Dynamic Loading, DYMAT, pp. 1649–1656.
Marchand, A., Duffy, J., 1988. An experimental study of the formation process of adiabatic shear bands in a structural steel. J. Mech. Phys. Solids 36 (3), 251–283.
Mason, J.J., Rosakis, A.J., Ravichandran, G., 1994. Full field measurements of the dynamic deformation field around a growing adiabatic shear band at the tip of a dynamically loaded crack or notch. J. Mech. Phys. Solids 42, 1679–1697.
Me-Bar, Y., Shechtman, D., 1983. On the adiabatic shear of Ti64 allistic targets. Mater. Sci. Eng. 53.
Meyer, L.W., Manwaring, S., 1986. In: Murr, L.E., Staudhammer, K.P., Meyers, M.A. (Eds.), Metallurgical Applications of Shock-Wave and High Strain Rate Phenomena. Marcel Dekker, NY.
Meyers, M.A., Xu, Y.B., Xue, Q., Perez-Prado, M.T., McNelly, T.R., 2003. Microstructural evolution in adiabatic shear localization in stainless steel. Acta Mater. 51, 1307–1325.
Molinari, A., 1997. Collective behavior and spacing of adiabatic shear bands. J. Mech. Phys. Solids 45 (9), 1551–1575.
Mott, N.F., 1947. Fragmentation of shell cases. Proc. R. Soc. Lond. 300, 300.
Nesterenko, V.F., Bondar, M.P., 1994. Localization of deformation in collapse of a thick walled cylinder. Combust. Explos. Shock Waves 30 (4), 500–505.
Nesterenko, V.F., Lazaridi, A.N., Pershin, S.A., 1989. Localization of deformation in copper by explosive compression of hollow cylinders. Fiz. Goreniya Vzryva 25 (4), 154–155.

Nesterenko, V.F., Meyers, M.A., Chen, H.C., LaSalvia, J.C., 1994. Controlled high-rate localized shear in porous reactive media. Appl. Phys. Lett. 65 (24), 3069–3071.
Olney, K.L., Chiu, P.H., Ribero Vairo, M.S., Higgins, A., Serge, M., Benson, D.J., Nesterenko, V.F., 2015. Influence of mesoscale properties on the mechanisms of plastic strain accomodation in plain strain dynamic deformation of concentric Ni–Al laminates. J. Appl. Phys. 117.
Olney, K.L., Chiu, P.H., Higgins, A., Serge, M., Weihs, T.P., Fritz, G.M., Stover, A.K., Benson, D.J., Nesterenko, V.F., 2014. Philos. Mag. 94, 3017–3035.
Osovski, S., Rittel, D., Landau, P., Venkert, A., 2012. Microstructural effects on adiabatic shear band formation. Scr. Mater. 66 (1), 9–12.
Rittel, D., et al., 1991. Experimental investigation of surface instabilities in cylindrical tensile metallic specimens. Acta Metall. Mater. 39, 719–724.
Rittel, D., Wang, Z.G., 2008. Thermo-mechanical aspects of adiabatic shear failure of AM50 and Ti6Al4V alloys. Mech. Mater. 40, 629–635.
Rittel, D., Wang, Z.G., Merzer, M., 2006. Adiabatic shear failure and dynamic stored energy of cold work. Phys. Rev. Lett. 96.
Rittel, D., Landau, P., Venkert, A., 2008. Dynamic recrystallization as a potential cause for adiabatic shear failure. Phys. Rev. Lett. 101.
Rogers, H.C., 1979. Adiabatic plastic deformation. Annu. Rev. Mater. Sci. 9.
Stokes, J.L., Nesterenko, V.F., Shlachter, J.S., Fulton, R.D., Indrakanti, S.S., Gu, YaBei, 2001. Comparative behavior of Ti and stainless steel in a magnetically-driven implosion at the Pegasus-II Facility. In: Staudhammer, K.P., Murr, L.E., Meyers, M.A. (Eds.), Proceedings of International Conference on Fundamental Issues and Applications of Shock-Wave and High-Strain-Rate Phenomena. Elsevier, Amsterdam, pp. 585–592.
Teng, X., Wierzbicki, T., Couque, H., 2007. On the transition from adiabatic shear banding to fracture. Mech. Mater. 39.
Wright, T.W., Okendon, H., 1996. A scaling law for the effect of inertia on the formation of adiabatic shear bands. Int. J. Plast. 12 (7), 927–934.
Xue, Q., Meyers, M.A., Nesterenko, V.F., 2002. Self organization of shear bands in titanium and Ti-6Al-4V alloy. Acta Mater. 50, 576–596.
Xue, Q., Meyers, M.A., Nesterenko, V.F., 2004. Self organization of shear bands in steel. Mater. Sci. Eng. A 384, 35–46.
Yang, Y., Zeng, Y., Gao, Z.W., 2008. Numerical and experimental studies of self-organization of shear bands in 7075 aluminum alloy. Mater. Sci. Eng. A 496, 291–302.
Yang, Y., Li, D.H., Zheng, H.G., Li, X.M., Jiang, F., 2009. Self organization behavior of shear bands in 7075-T73 and annealed aluminum. Mater. Sci. Eng. A 527, 344–354.
Zener, C., Hollomon, J.H., 1943. Effect of strain rate upon plastic flow of steel. J. Appl. Phys., 22–32.
Zhou, M., Rosakis, A.J., Ravichraden, G., 1996a. Dynamically propagating shear bands in impact-loaded prenotched plates – I experimental investigations of temperature signatures and propagation speed. J. Mech. Phys. Solids 44 (6), 981–1006.
Zhou, M., Rosakis, A.J., Ravichraden, G., 1996b. Dynamically propagating shear bands in impact-loaded prenotched plates – II numerical simulations. J. Mech. Phys. Solids 44 (6), 1006–1032.